



1
2
3
4
5
6
7
8
9
10
11
12
13
14
15
16
17
18
19
20
21
22
23

Development of a balloon-borne instrument for CO₂ vertical profile observations in the troposphere

**Mai Ouchi¹, Yutaka Matsumi^{1*}, Tomoki Nakayama², Kensaku Shimizu³, Takehiko Sawada³,
Toshinobu Machida⁴, Hidekazu Matsueda⁵, Yousuke Sawa⁵, Isamu Morino⁴, Osamu Uchino⁴,
Tomoaki Tanaka^{6,a}, Ryoichi Imasu⁷**

¹Institute for Space-Earth Environmental Research and Graduate School of Science, Nagoya
University, Furo-cho, Chikusa-ku, Nagoya 464-8601, Japan

²Graduate School of Fisheries and Environmental Sciences, Nagasaki University, 1-14, Bunkyo-machi,
Nagasaki, Nagasaki 852-8521 Japan

³Meisei Electric co., Ltd., 2223 Naganumamachi, Isesaki-shi, Gunma 372-8585, Japan

⁴National Institute for Environmental Studies, 16-2 Onogawa, Tsukuba, Ibaraki 305-8506 Japan

⁵Meteorological Research Institute, Japan Meteorological Agency, 1-1 Nagamine, Tsukuba, Ibaraki
305-0052, Japan

⁶Japan Aerospace Exploration Agency Earth Observation Research Center, 2-1-1, Sengen, Tsukuba,
Ibaraki 305-8505, Japan

⁷Atmosphere and Ocean Research Institute, The University of Tokyo, 5-1-5, Kashiwanoha, Kashiwa,
Chiba 277-8568, Japan

^anow at: NASA Ames Research Center, Moffett Field Mountain View CA 94035, USA

Corresponding author: matsumi@nagoya-u.jp



24 **Abstract**

25 A novel, practical observation system for measuring tropospheric carbon dioxide (CO₂)
26 concentrations using a non-dispersive infrared analyzer carried by a small helium-filled balloon (CO₂
27 sonde), has been developed for the first time. Onboard calibrations, using CO₂ standard gases, is
28 possible to measure the vertical profiles of atmospheric CO₂ accurately with a 240-400 m altitude
29 resolution. The standard deviations (1σ) of the measured mole fractions in the laboratory experiments
30 using a vacuum chamber at a temperature of 298 K were approximately 0.6 ppm at 1010 hPa and 1.2
31 ppm at 250 hPa. Compared with in situ aircraft data, although the difference up to the altitude of 7 km
32 was 0.6 ± 1.2 ppm, this bias and difference were within the precision of the CO₂ sonde. In field
33 experiments, the CO₂ sonde detected an increase in CO₂ concentration in an urban area and a decrease
34 in a forested area near the surface. The CO₂ sonde was shown to be a useful instrument for observing
35 and monitoring the vertical profiles of CO₂ concentration in the troposphere.

36

37



38 1. Introduction

39 Atmospheric carbon dioxide (CO₂) is one of the most important anthropogenic greenhouse gases
40 for global warming. Certain human activities, such as fossil fuel combustion, cement production, and
41 deforestation are the major cause of atmospheric CO₂, making the global average concentration of
42 atmospheric CO₂ to increase from 280 ppm before the Industrial Revolution to 400.0 ppm in 2015
43 (World Meteorological Organization, WMO 2016). Over the last 10 years, the rates of atmospheric
44 CO₂ increase is measured at 2.21 ppm yr⁻¹ (WMO 2016). Atmospheric CO₂ is measured by ground-
45 based stations and ships using the flask sampling and continuous instrument methods such as non-
46 dispersive infrared absorption (NDIR) (Tanaka et al. 1983, Hodgkinson et al. 2013) and cavity ring-
47 down spectroscopy (CRDS) (Winderlitch et al. 2010). A network of ground-based Fourier transforms
48 spectrometers (FTS), that record the direct solar spectra in the near-infrared spectral region (Total
49 Carbon Column Observing Network, TCCON), is used to observe the column-averaged mole fraction
50 of CO₂ in dry air (total column XCO₂) (Wunch et al. 2011). These observations have provided an
51 extensive information, regarding the distribution and temporal variation of CO₂ in the atmosphere
52 (Pales and Keeling, 1965; Conway et al. 1988; Komhyr et al. 1989; Tans et al. 1989; Conway et al.
53 1994). Moreover, atmospheric CO₂ measurements data are useful for estimating CO₂ fluxes at the
54 surface through inverse modeling (Gurney et al. 2004; Baker et al. 2006). Due to the limited number
55 of observation sites and the limitations of their altitudinal range, a large degree of uncertainty in the
56 current estimates of the regional CO₂ sources and sinks is noted (Gurney et al. 2002). More
57 atmospheric CO₂ measurements are needed to reduce the uncertainties in CO₂ fluxes estimation using
58 an inverse modeling.

59 To address the issues with insufficient CO₂ observational data, satellite remote sensing techniques
60 have been used to investigate the CO₂ distribution on a global scale (Chédin et al. 2002; Crevoisier et
61 al. 2004; Dils et al. 2006). The Greenhouse Gases Observing SATellite (GOSAT), which measures the
62 short wavelength infrared (SWIR) spectra of sunlight reflected by the earth's surface with a Fourier



63 transform spectrometer and obtains the total column XCO₂, has been in operation since early 2009
64 (Yokota et al. 2009; Yoshida et al. 2011; Morino et al. 2011). Since 2014, the Orbiting Carbon
65 Observatory-2 (OCO-2) satellite has also measured the IR spectra of the surface reflected sunlight
66 with a diffraction grating spectrometer and obtains total column XCO₂ (Eldering et al. 2017). However,
67 these satellite observations provide only nadir total column XCO₂, and do not measure the vertical
68 distributions of CO₂ concentrations, as the observed spectra of the surface-reflected sunlight do not
69 provide enough information to determine the vertical distributions. Furthermore, the satellites overpass
70 a specific earth-based target once several days only at about noon in the solar time because of their
71 sun-synchronous orbits.

72 The altitude distributions of CO₂ concentrations has been measured using other techniques. For
73 instance, tall towers measure vertical profiles of CO₂ near the ground (Bakwin et al. 1992, Inoue and
74 Matsueda, 2001; Andrews et al. 2014). CO₂ vertical profiles up to 10 km near the airports have been
75 observed by the equipment installed by the commercial airlines, such as the Comprehensive
76 Observation Network for TRace gases by Airliner (CONTRAIL program) (Machida et al. 2008;
77 Matsueda et al. 2008). Measurements by equipment installed on chartered aircrafts have also been
78 undertaken, which include the High-performance Instrumented Airborne Platform for Environmental
79 Research (HIAPER), Pole-to-Pole Observations (HIPPO) program up to 14 km in the altitude spanning
80 the Pacific from 85° N to 67° S (Wofsy et al. 2011), the NIES/JAXA (National Institute of
81 Environmental Studies and Japan Aerospace eXploration Agency) program at an altitude from 2 to 7
82 km (Tanaka et al. 2012), and the NOAA/ESRL Global Greenhouse Gas Reference Network Aircraft
83 Program (Sweeney et al. 2015). Although these aircraft measurements provided the vertical profiles
84 of CO₂ concentrations, they had the short-term observation campaigns in the limited areas or
85 measurements around a limited number of large airports used by the commercial airlines. The
86 continuation and expansion of airborne measurement programs for CO₂ and related tracers are
87 expected to enhance the estimation of the global carbon cycling greatly (Stephens et al., 2007).



88 Atmospheric CO₂ observations using balloons, to select specific locations unless prohibited or
89 restricted by aircraft flight paths, are useful for solving the issues associated with the sparseness of
90 CO₂ vertical data. Balloon-borne observations of stratospheric CO₂ are previously conducted by other
91 studies. For instance, stratospheric air sampling was conducted using a cryogenic sampler onboard
92 balloons once a year from 1985 to 1995 over the northern part of Japan (Nakazawa et al. 1995).
93 Balloon-borne near-infrared tunable diode laser spectrometers have been developed to provide in situ
94 data for CO₂ in the stratospheric atmosphere (Durry et al. 2004; Joly et al. 2007, Ghysels et al. 2012).
95 Furthermore, two in situ CO₂ analyzers adopting the NDIR technique, using a modified commercial
96 detector for stratospheric measurements, have been developed for deployment on the NASA ER-2
97 aircraft and on a balloon (Daube et al. 2002). These balloon borne instruments described above were
98 specially designed to measure CO₂ concentrations in the stratosphere.

99 Observation of the CO₂ vertical distribution in the troposphere is essential because the uncertainties
100 in the estimated fluxes, using the inverse method, can be attributed to the inaccurate representations of
101 the atmospheric processes in transport models. Misrepresentation of vertical mixing by the transport
102 models, particularly inside of the boundary layer, which is the layer closest to the ground where CO₂
103 is taken up and released, is one of the dominant causes of the uncertainty in CO₂ flux estimation
104 (Stephens et al. 2007; Ahmadov et al. 2009). Recently, the observation of tropospheric CO₂ was
105 conducted, using a lightweight unmanned aerial vehicle, such as a kite plane, with a commercial NDIR
106 instrument. CO₂ profiles were observed in and above the planetary boundary layer up to 2 km to
107 investigate the temporal and spatial variations of CO₂ (Watai et al. 2006). A passive air sampling
108 system for atmospheric CO₂ measurements, using a 150 m long stainless-steel tube called an AirCore
109 was developed (Karion et al. 2010). The AirCore mounted on an airplane or a balloon ascends with
110 evacuating inside of the tube to a high altitude of 30 km at flight maximum, then, collecting ambient air
111 by pressure changes along a decrease in altitude. The sampled air in the tube is analyzed with the
112 precision of 0.07 ppm for CO₂ indicated as one standard deviation in the laboratory and the vertical



113 profile of CO₂ is obtained.

114 In the present study, we have developed a practical CO₂ sonde system that can measure in situ CO₂
115 vertical profiles in the atmosphere from the ground to altitudes up to about 10 km with a 240-400 m
116 altitude resolution by using a small-sized balloon. Although the sonde system is thrown away after
117 every flight due to the difficulties associated with recovery, the sonde systems are easily prepared with
118 a relatively low cost. We have tested the sonde flight experiments more than 20 times in Japan. The
119 CO₂ sonde developed has the following advantages, compared with other measurement techniques
120 described above: (1) its cost of operation is low and the flight permission is easy to obtain from the
121 authorities as compared with the aircraft observations; (2) the CO₂ sonde can be easily carried to the
122 launch sites since the instrument is light; (3) a limited amount of power is required for the operation;
123 (4) it can generally be launched at any time; and (5) the meteorological data are obtained
124 simultaneously with CO₂ profile data. In this study, the design of our novel CO₂ sonde and the results
125 of the comparison experiments with aircraft measurements are described. The target accuracy and
126 precision in the measurements with the CO₂ sonde are below about 1 ppm CO₂ mole fraction in the
127 atmosphere of 400 ppm CO₂, preferable for carbon cycle studies (e.g. Maksyutov et al. 2008). The
128 developed CO₂ sonde system attained virtually all the targets from the ground to an altitude of about
129 10 km.

130 Inai et al. (2018) measured vertical profiles of CO₂ mole fraction in the equatorial eastern and
131 western Pacific in February 2012 and February–March 2015, respectively, by using our novel CO₂
132 sondes which are described in this report. They found that the 1–10 km vertically averaged CO₂ mole
133 fractions lie between the background surface values in the Northern Hemisphere (NH) and those in the
134 Southern Hemisphere (SH) monitored at ground-based sites during these periods. Their study showed
135 that the combination of CO₂ sonde measurements and trajectory analysis, taking account of convective
136 mixing, was a useful tool in investigating CO₂ transport processes.

137



138 **2. Materials and methods**

139 **a. Design of the CO₂ sonde**

140 Many severe restrictions are noted for the operation of balloon-borne CO₂ sondes. First, the weight
141 of the CO₂ sonde package should be less than about 2 kg, based on the legal restriction by the US FAA
142 (Federal Aviation Administration) and by the Japanese aviation laws for the payload weight of 2.721
143 kg for unmanned free balloons. Balloon systems heavier than the above regulation weight are not
144 useful for the frequent flights because the flight permission from the authorities is much more difficult
145 to obtain, and the additional safety requirements are more expensive. The balloon system is thrown
146 away in the ocean after each flight due to a long-distance transportation (100 km or more to the east)
147 by strong westerly winds in the upper atmosphere of mid-latitude area. This is done to avoid the
148 accidents associated with a falling onto the urban areas, resulting in high recovery costs. Therefore,
149 the cost of the CO₂ sonde system should be low for frequent observations. The non-recovery system
150 implies that every instrument should perform consistently.

151 In this study the NDIR technique was adopted for a detection of CO₂ concentrations. The NDIR
152 CO₂ measurement techniques have been widely used in many places such as WMO/GAW (Global
153 Atmosphere Watch) stations. Our target instrumental accuracy and precision of approximately 1 ppm
154 are less stringent than those of the ground-based instruments (± 0.1 ppm) used at the WMO/GAW
155 stations (WMO, 2016). However, the surrounding conditions for the instrument are substantially
156 severe during the flight experiments, as the pressure changes from 1,000 to 250 hPa and the
157 surrounding temperature changes from 300 to 220 K during flights from the surface to an altitude of
158 10 km in about 60 min.

159 In the NDIR technique for CO₂ measurements, the IR emission from a broadband wavelength source
160 is passed through an optical cell and two filters, and then the light intensities are detected by two IR
161 detectors. The one optical filter covers the whole absorption band of CO₂ around 4.3 μm , while the
162 other covers a neighboring non-absorbed region around 4.0 μm . provided that the chosen active and



163 reference channel filters do not significantly overlap with the absorption bands of other gas species
164 present in the application. (Hodgkinson et al., 2013).

165 The Beer–Lambert Law is expressed by Eq. (1), defining the light intensity in the absence of CO₂
166 in the cell as I_0 and the light intensity in the presence of CO₂ in the cell as I ,

$$167 \quad \frac{I}{I_0} = \exp(-\varepsilon CL) \quad (1),$$

168 where C is the CO₂ concentration in molecules cm⁻³, L is the optical path length in cm, and ε is
169 the absorption cross-section in cm² molecule⁻¹. Using the relationship of $C = XP (k_B T)^{-1}$, where X
170 is the CO₂ mole fraction and P is the pressure of dehumidified ambient air, and the approximation
171 of $\exp(-\varepsilon CL) = 1 - \varepsilon CL$, under the condition of $\varepsilon CL \ll 1$, Eq. (1) is rewritten as:

$$172 \quad \frac{(I_0 - I)}{P} = X \frac{I_0 \varepsilon L}{k_B T_c} \quad (2),$$

173 where T_c is the sample air temperature in the sensor cell and k_B is the Boltzmann constant. With a 120
174 mm long absorption cell, the absorption intensity is approximately 3% at 400 ppm CO₂ with our CO₂
175 NDIR system, i.e., $\varepsilon CL \approx 0.03$ and the approximation of $\exp(-\varepsilon CL) = 1 - \varepsilon CL$ are well fitted. The
176 values of $[I(4.0) - I(4.3)]$ were used instead of $(I_0 - I)$ to obtain the CO₂ mole fraction values in
177 the NDIR measurements, where $I(4.0)$ and $I(4.3)$ were the signal intensities at the 4.0 μm
178 wavelength for background measurements and the 4.3 μm wavelength for CO₂ absorption
179 measurements, respectively. Thus, the value of $[I(4.0) - I(4.3)]/P$ is thus proportional to the CO₂
180 mole fraction X in the optical cell. The proportional constant is usually determined by the
181 measurements of the standard gases. In the NDIR measurements at the ground WMO/GAW stations,
182 carbon dioxide mole fractions are referenced to a high working standard and a low working standard
183 and are determined by the interpolations of the signals with the two standards, and the calibration with
184 the two standard gases are carried out every 12 h (Fang et al., 2014).

185

186 **b. System configuration of the CO₂ sonde system**



187 A schematic diagram and photograph of the CO₂ measurement instrument are shown in Fig. 1. The
188 CO₂ sonde has three inlets installed for ambient air and two calibration gases with mesh filters (EMD
189 Millipore, Millex-HA, 0.45 μm pore size) to remove the atmospheric particles. Three solenoid valves
190 (Koganei, G010LE1-21) were used to switch the gas flow to the CO₂ sensor. A constant-volume piston
191 pump with a flow rate of 300 cm³ min⁻¹ (Meisei Electric co., Ltd.), which is originally used for
192 ozonesonde instruments, directed the gas flows from the inlets through the solenoid valves into a
193 dehumidifier, a flow meter, and a CO₂ sensor. The absolute STP (standard temperature and pressure)
194 flowrate decreased with a decrease in pressure. Since the exit port of the CO₂ sensor was opened to
195 the ambient air, the pressure of dehumidified outside air and calibration gases in the absorption cell
196 were equal to the ambient pressure during the flight. Next to the pump, the gases were introduced to a
197 glass tube filled with the magnesium perchlorate grains (dehumidifier) installed upstream to the CO₂
198 sensor to remove the water vapor. Fabric filters were installed on both ends of the dehumidifier, and a
199 mesh filter was installed downstream of the dehumidifier to prevent the CO₂ sensor from the incursion
200 of magnesium perchlorate grains to the optical cell.

201 The infrared absorption cell consisted of a gold-coated glass tube, a light source, and a photodetector.
202 The light source (Helioworks, EP3963) consisted of a tungsten filament with a spectral peak intensity
203 wavelength of approximately 4 μm. The light from the source passed through a gold-coated glass tube
204 (length 120 mm, and inside diameter 9.0 mm). The commercial CO₂ NDIR photodetector (Perkin-
205 Elmer TPS2734) had two thermopile elements, one of which was equipped with a band-pass filter at a
206 wavelength of 4.3 μm for the measurement of the CO₂ absorption signal, whereas the other was
207 equipped with a band-pass filter at a wavelength of 4.0 μm for the measurement of the background
208 signal. The signals from the sensors were amplified by an operational amplifier and converted to 16
209 bit digital values by an A/D convertor. The signal intensities of the detectors at 4.0 and 4.3 μm without
210 CO₂ gas were set to the equal levels by adjusting the amplification factors in the laboratory. The electric
211 power for the CO₂ sensor, pump, and valves was supplied through a control board using three 9 V



212 lithium batteries, lasted for more than 3 h during the flight. The control board connected to the
213 components regulated the measurement procedures, such as switching the solenoid valves and
214 processing the signal. As shown in Fig. 1, the measurement system has an expanded polystyrene box
215 molded specially to settle the optical absorption cell, electronic board, pump, battery and other
216 components.

217

218 **c. Calibration gas package**

219 Under the wide ranges of temperature and pressure conditions, the CO₂ sensor signal was unstable,
220 and the calibration of the CO₂ sensor only on the ground before launch was insufficient to obtain the
221 precise values of the CO₂ concentrations. To solve this problem, an in-flight calibration system was
222 incorporated into the CO₂ sonde. A calibration gas package was attached to the CO₂ sonde for the in-
223 flight calibration, as shown in Fig. 2. The calibration gas package consisted of two aluminum coated
224 with polytetrafluoroethylene (PTFE) bags (maximum volume: 20 L), containing reference gases with
225 low (~370 ppm) and high (~400 ppm) CO₂ concentrations. In each bag, ~8 L (STP) of the reference
226 gas was introduced from standard CO₂ gas cylinders just before launch. Since the gas bags were soft,
227 their inner pressures were equal with the ambient air pressures during the balloon flight. The gas
228 volumes in the bags increased with the altitude during the ascent of the balloon due to a decrease in
229 the ambient pressure, while the reference gases were consumed during the calibration procedures. The
230 optimum amounts of gas in the bags were determined by both the ascending speed of the balloon and
231 the consumption rate to avoid the bursting of the bags and exhaustion of the gases. The CO₂
232 concentrations of the reference gases in the bags were checked by the NDIR instrument (LICOR, LI-
233 840) before launching. Thereafter, approximately 6 L of the reference gas was left in each bag for a
234 subsequent in-flight calibration. The change in the CO₂ mole fraction in the bags was less than 1 ppm
235 over a 3 days period, which was negligible over the observations time during the balloon flight. All
236 measurements were reported as dry-air mole fractions relative to the internally consistent standard
237 scales maintained at Tohoku University (Tanaka et al. 1987; Nakazawa et al. 1992).



238 Since the gas exit port of the optical absorption cell was opened to the ambient air, the cell pressure
239 was equalized with the ambient pressure for measuring both the ambient air and two standard gases.
240 During the balloon-borne flights, the temperatures inside the CO₂ sonde package were measured with
241 thermistors. The temperature inside the CO₂ sonde package gradually decreased by approximately 5
242 K, from 298 K on the ground to 293 K at an altitude of 10 km during the flights. Probably due to the
243 polystyrene box, and the heat produced by the NDIR lamp, pump and solenoid valves, temperature
244 inside the sonde package remained virtually constant in spite of low ambient temperatures at high
245 altitudes (~220 K). Within one measurement cycle time (160 s) with the standard gases, the
246 temperature change was less than 0.4 K in the sonde package. The temperatures of the sample gas in
247 the tube just before the inlet of the CO₂ NDIR cell were also measured using a thin wire thermistor,
248 commonly used for ambient temperature measurement in GPS sonde equipment with a quick response
249 time (shorter than 2 s). The gas temperature change was negligible at the valve change timings between
250 the standard gas and ambient air (< 0.1 K). The result indicated that the gas temperatures were
251 relatively constant after passing through the valves, pump, dehumidifier cell, and piping for both the
252 standard gases and ambient air.

253 The performances of the CO₂ sonde instruments were checked before the balloon launching since
254 the CO₂ sonde systems were not recovered after the launch experiments were performed. For about 60
255 min. before the launch, the values of $[I(4.0) - I(4.3)]/P$ were measured with the valve cycles (each
256 step 40 s, total 160 s) for two standard gas packages (~370 ppm and ~400 ppm) for calibration and one
257 intermediate concentration gas package (~385 ppm) as a simulated ambient gas sample.

258

259 **d. Total sonde system**

260 The CO₂ sonde was equipped with a GPS radiosonde (Meisei Electric co., Ltd., RS-06G). The
261 balloon carried the instrument packages in the altitude with measuring CO₂ and meteorological data
262 (GPS position and time, temperature, pressure, and humidity). The CO₂ sonde transmitted those data



263 to a ground receiver (Meisei Electric co., Ltd., RD-08AC) at 1 s intervals, thus it was unnecessary to
264 recover the CO₂ sonde after the balloon burst. Figure 2 showed an overall view of the CO₂ sonde
265 developed in this study, which consisted of a CO₂ measurement package, a calibration gas package, a
266 GPS radiosonde, a balloon, and a parachute. The total weight of the CO₂ sonde was 1700 g, including
267 the GPS radiosonde (150 g), CO₂ measurement package (1000 g), and calibration gas package (550 g).
268 The dimensions of the CO₂ measurement package were width (W) 280 mm × height (H) 150 mm ×
269 depth (D) 280 mm. The size of the calibration gas package was W 400 mm × H 420 mm × D 490 mm.

270 The CO₂ sonde system was flown by a 1200 g rubber balloon (Totex). The ascending speed was
271 around 4 m / s by controlling the helium gas amount in the rubber balloon and checking the buoyancy
272 force. In practice, it was difficult to precisely control the ascending speed of the balloon, and the actual
273 resulting speeds were in the range of 3 - 5 m s⁻¹. This corresponds to the height resolution of
274 approximately 240–400 m for the measurements of the CO₂ vertical profiles.

275 Ascending speed slower than 3 m s⁻¹ can lead to a collision with a nearby tree and building, result
276 in equipment falling in the urban areas. With faster ascending speeds, the altitude resolution of the
277 measurements decreased and the gas standard bag became full and the pressure inside the gas bags
278 became higher than the ambient pressure because of the lower ambient pressures at higher altitudes.
279 The high pressure inside the gas bag resulted in the fast flow speed in the optical absorption cell of
280 NDIR, which shifted the signal values for the pressurized gas sample. Since pressure relief valves for
281 the bags did not work at low pressures at high altitudes, we did not use the pressure relief valve for the
282 standard gas bags. When the ascending speed was low, the standard gas bags became empty since they
283 were consumed by the in-flight calibration procedures during the long ascending time. Since the
284 measurements after the over-pressurization or the exhaustion of the reference gas bag are useless, this
285 technical problem determines the upper limit (10 km) of altitude for the measurements in this study.
286 Based on our experiences, this problem generally occurred at an altitude above approximately 10 km.
287



288 e. Data processing procedures

289 Since the surrounding conditions of the sonde change significantly during the ascending period,
290 the NDIR measurement system is calibrated with the two standard gases at every altitudes. However,
291 since the balloon-borne instrument is only equipped with one NDIR absorption cell and the balloon
292 ascends continuously, it is not possible to measure the ambient air sample and the two standard gases
293 at the same time and at the same altitude. Therefore, the measurement cycle during the flights
294 consisted of the following steps: (1) low concentration standard gas, (2) ambient air, (3) high
295 concentration standard gas, and (4) ambient air. The measurement time for each step was 40 s. At
296 switching timings of the valve cycles, the signal became stable within 10 s, and the averages of residual
297 30-s period signals were used for the calculation of the CO₂ mole fractions. Since the gas exit port of
298 the NDIR optical absorption cell was opened to the ambient air, the cell pressure was equalized with
299 the ambient pressure. During the period of the 40 s gas change, the pressure would change about 2 %
300 when the ascending speed of the balloon was 4 m s⁻¹. The temperature of the ambient air and standard
301 gas samples at the inlet port of the optical cells was measured and found to be constant during each
302 cycle of the calibration procedure.

303 Figure 3 shows an example of the raw data obtained from the CO₂ sonde experiment. Figure 3
304 presents the plots of the values of $[I(4.0) - I(4.3)]/P$ against the altitude, where $I(4.0)$ and $I(4.3)$
305 are the signal intensities at the wavelength of 4.0 μm for background measurements and the 4.3 μm
306 wavelength for CO₂ absorption measurements, as obtained by the NDIR CO₂ sensor on the balloon,
307 and P is the ambient atmospheric pressure obtained by the GPS sonde data and pressure
308 measurements on the ground.

309 The values of $[I(4.0) - I(4.3)]/P$ are proportional to the CO₂ mole fraction X according to the
310 Beer-Lambert law as expressed by Eq. (2). By using the values of $[I(4.0) - I(4.3)]/P$, we can
311 compensate for the pressure change to determine the CO₂ concentration. As shown in Fig. 3, the
312 differences in the $[I(4.0) - I(4.3)]/P$ values between the low and high standard gases remained



313 relatively constant while ascending to the higher altitudes. However, the $[I(4.0) - I(4.3)]/P$ values
314 for the each standard gas did not change linearly but sometimes displayed some curvatures as shown
315 in Fig. 3. This may be due to the differences between the baseline drift of the two sensors at 4.3 μm
316 and 4.0 μm in the NDIR detector. Since the measurements were performed alternately for the standard
317 gases and the ambient air with the NDIR cell and are not performed simultaneously, the values for the
318 standard gas signals at the time of the ambient air measurement was estimated. Therefore, the cubic
319 spline fitting curves for the observation points of the 30 s average values (red circles in Fig. 3) of the
320 same standard gas were used to obtain the low and high calibration points for the calculation of the
321 mole fractions in the ambient air. In Fig. 3, the cubic spline fitting curves are represented by the red
322 curves, and the estimated values for the standard gases at the ambient gas measuring time are
323 represented by the small black dots on the cubic spline curves, which are used for the interpolation to
324 determine the ambient air concentrations. Linear line fitting between the standard gas values did not
325 work well because the connection lines of the values sometimes displayed curvatures as shown in Fig.
326 3. Since there were in-phase fluctuations in the $I(4.0)$ and $I(4.3)$ signals during the flights, the
327 subtraction of $[I(4.0) - I(4.3)]$ could partly improve the signal-to-noise ratios by canceling in-phase
328 fluctuations with each other.

329

330 3. Results and discussion

331 a. Laboratory tests

332 Since the linear interpolation method for the $[I(4.0) - I(4.3)]/P$ values was used to determine the
333 ambient air CO_2 mole fractions in the balloon-borne experiments, the deviations from the linear
334 interpolation process were also investigated. The measurements of various mole fractions gas samples
335 in the laboratory indicated that the linear interpolation error with the two standard gas packages (~370
336 ppm and ~400 ppm) was less than 0.2 ppm in the range between 360 and 410 ppm. Figure 4 shows the
337 measurement results of the NDIR cell developed in this study at various CO_2 mole fractions. The outlet



338 port of the NDIR system was connected to the commercial CO₂ instrument (LICOR, LI-840A) as a
339 standard device, and the two instrument simultaneously measure the sample gas at 1010 hPa. The
340 standard gases of 365 and 402 ppm were used for the calibration, and the mixtures of the standard
341 gases were used for the samples. This indicated the values of $[I(4.0) - I(4.3)]/P$ of the system were
342 proportional to the mole fraction of CO₂. This type of experiment could not be performed at low
343 pressures, since we did not have a standard device which can be operated under low pressures.

344 Figure 5 shows the results of an experiment using a vacuum chamber in the laboratory, where the
345 flight pressure conditions were simulated and the performances of the CO₂ sonde instruments was
346 evaluated. The temperature inside the chamber was not controlled and was about 298 K. In the actual
347 flights, the temperature inside the sonde package did not change more than 5 K. The CO₂ sonde system
348 and two standard gas packages were placed in the vacuum chamber. The chamber was filled with the
349 mole fraction sample gas of 377.3 ppm before the pumping. The pressure of the chamber was gradually
350 and continuously decreased using a mechanical pump from 1010 hPa (ground surface pressure) to 250
351 hPa (about 10 km altitude pressure) over 60 min, corresponded to a balloon ascending speed of 3 m/s
352 in actual flights, whereas the sample gas was slowly and continuously supplied to the chamber. The
353 values $[I(4.0) - I(4.3)]/P$ were measured for the two standard gas packages, and the sample gas with
354 the valve cycles (each step 40 s, total 160 s) as described in the previous section. The mole fractions
355 of the sample gas in the chamber were calculated by the interpolation of the signals for the two standard
356 gases. The 30 s signals 10 s after the valve changes were used for the interpolation calculations to
357 avoid the incomplete gas exchanges in the NDIR optical cell. The black circle in Fig. 5 indicates the
358 sample gas mole fraction obtained from the linearly interpolated standard gas signals in each
359 calibration cycle. The vertical error bar in Fig. 5 indicates the square-root of the sum of squares for the
360 standard deviations of the sample and standard gas signals at each step. The errors in the CO₂ mole
361 fractions were estimated to be 0.6 ppm at 1010 hPa and 1.2 ppm at 250 hPa using the calibration cycles.
362 The results in Fig. 5 indicated that the determination of the sample gas concentration using the linear



363 interpolation with the standard gases was appropriate within the error, when the pressure continuously
364 decreased from 1000 to 250 ppm over 60 min.

365 When the CO₂ sonde instrument was inclined and vibrated in the laboratory, the fluctuations in the
366 signals were observed. The quantitative correlation between the signal fluctuation intensities and
367 acceleration speed, measured by a 3-dimensional acceleration sensor, was investigated, but no distinct
368 correlation was detected. However, the in-flight calibration system partly solved this problem by taking
369 the signal difference of $[I(4.0) - I(4.3)]$ and also by measuring alternately the two standard gases
370 every 40 s during the balloon flights.

371 The temperature characteristics of the CO₂ sensor were also investigated by changing the sensor cell
372 block temperature from 273 to 323 K at the pressure of ~1010 hPa, using a heater in the laboratory.
373 The laboratory experiment related to the temperature dependence suggested that the measurement error
374 is less than 0.2 ppm due to the temperature change during one valve cycle (160 s) in the balloon-borne
375 experiments.

376 In principle, the absorption intensities $(I_0 - I)$ in the NDIR measurements are proportional to the
377 absolute CO₂ concentrations in the sample air in the absorption cell. Therefore, at higher altitudes
378 where the pressures were lower, the values of $[I(4.0) - I(4.3)]$ were smaller and the signal-to-noise
379 ratios of $[I(4.0) - I(4.3)]/P$ decreased. The error of the CO₂ mole fractions of 1.2 ppm at 250 hPa
380 corresponds to an absolute CO₂ concentration of 3.2×10^{13} molecule cm⁻³. The equivalent altitude for
381 this value was 90 km with a CO₂ molar fraction of 400 ppm. As described previously, the purpose of
382 CO₂ balloon observations is to measure the CO₂ mole fraction within a 1 ppm errors in the atmospheres
383 around 400 ppm CO₂. The upper limit of the altitude for the observations with the developed CO₂
384 sonde is considered to be ~10 km. Furthermore, as described in section 2d, the problems of the vacancy
385 or over-pressure in the standard gas bags took place around 10 km altitudes, which resulted in large
386 errors. This also practically determines the upper altitude limit for CO₂ sonde observations.

387



388 **b. Comparison with aircraft data**

389 Two types of aircraft measurement data, the NIES/JAXA chartered aircraft and the CONTRAIL
390 data, were used for comparison with the CO₂ sonde measurement data. The NIES/JAXA chartered
391 aircraft measurements were conducted on the same days as the CO₂ sonde observations (January 31st,
392 2011 and February 3rd, 2011). The chartered aircraft observations were performed as a part of the
393 campaign for validating the GOSAT data and calibrating the TCCON FTS data at Tsukuba (36.05°N,
394 140.12°E) (Tanaka et al., 2012). The chartered aircraft data were obtained using an NDIR instrument
395 (LICOR LI-840) that had a control system of constant pressure and had the uncertainty of 0.2 ppm.
396 On both January 31st and February 3rd, the chartered aircraft measured the CO₂ mole fractions during
397 descent spirals over Tsukuba and Kumagaya (Fig. 6). Because the air traffic was strictly regulated near
398 the Haneda and Narita international airports, the aircraft observations at altitudes above 2 km over
399 Tsukuba were prohibited. Therefore, the descent spiral observations were conducted over Kumagaya
400 at altitudes of 7–2 km and over Tsukuba at altitudes of 2–0.5 km. Tsukuba is located approximately 20
401 km northeast of Moriya, whereas Kumagaya is located approximately 70 km northwest of Moriya.

402 Seven profiles based on the CONTRAIL measurements, obtained during the ascent and descent of
403 aircrafts over Narita airport and had passage times close to the CO₂ sonde observations, were available
404 within two days after or before the dates of the CO₂ sonde measurements (Table 1). The CO₂ sonde
405 observations were conducted on January 31st and February 3rd, 2011 from Moriya. One set of
406 CONTRAIL data, obtained from the flight from Hong Kong to Narita (data set name: 11_060d), was
407 available on January 31st, but no CONTRAIL data were available for February 3rd. Therefore, the
408 CONTRAIL data, obtained from the flight from Hong Kong to Narita on February 2nd (data set name:
409 11_062d), were used for comparison with the February 3rd CO₂ sonde data. Figure 6 also shows the
410 CONTRAIL 11_060d and 11_062d flight paths and the CO₂ sonde launched at Moriya on January 31st
411 and February 3rd, 2011. On January 31st, the flight time of the CONTRAIL 11_060d over the Narita
412 airport and the launch time of the CO₂ sonde at Moriya were relatively close to one another. The flight



413 path of the CONTRAIL 11_062d data on February 2nd, 2011 was close to that of the CO₂ sonde on
414 February 3rd, 2011 and both observations were conducted in the early afternoon. The CONTRAIL
415 data referred in the present study was obtained using the Continuous CO₂ Measuring Equipment
416 (CME) located onboard commercial airliners (Machida et al. 2008; Matsueda et al. 2008). The typical
417 measurement uncertainty (1σ) of the CME has been reported as 0.2 ppm (Machida et al. 2008).

418 Figure 7 shows the vertical profiles of CO₂ observed by the CO₂ sonde at Moriya, the chartered
419 aircraft at Kumagaya and Tsukuba, and the CONTRAIL over the Narita airport on January 31st, 2011.
420 The overall vertical distribution of the CO₂ sonde data resembled with those of the chartered aircraft.
421 The vertical profiles of the CONTRAIL 11_060d flight on January 31st at the 5.3–6.8 km altitude
422 range consisted of the missing data because of the CME calibration period.

423 Figure 8 shows the comparison of the CO₂ vertical profiles obtained by the CO₂ sonde over Moriya,
424 NIES/JAXA chartered aircraft over Kumagaya and Tsukuba on February 3rd, 2011, and the
425 CONTRAIL on February 2nd, 2011 over Narita. The shape of the vertical profile obtained by the
426 chartered aircraft on February 3rd resembled that obtained by the CO₂ sonde, although the profile from
427 the chartered aircraft was shifted to the lower CO₂ concentration side compared to that of the CO₂
428 sonde.

429 Table 2 lists the comparisons of the CO₂ concentrations measured by the balloon CO₂ sonde and
430 NIES/JAXA chartered aircraft on January 31st and February 3rd, 2011. The averaged values of the
431 aircraft measurement over the range of each balloon altitude ± 100 m are listed in Table 2, since the
432 altitude resolution of the aircraft measurements is higher than that of the CO₂ sonde. From the February
433 3rd measurements, the height of the boundary layer around an altitude of 1 km was different between
434 the CO₂ sonde and the NIES/JAXA aircraft measurements as shown in Fig. 8. Therefore, the data
435 below 1 km on February 3rd are not included in Table 2. From the data on January 31st, the averaged
436 value of the differences between the CO₂ sonde and the NIES/JAXA aircraft was relatively small (0.42
437 ppm), which corresponded to the bias of the measurements. The standard deviation of the differences



438 was 1.24 ppm. From the February 3rd data, the bias was large (1.41 ppm), whereas the standard
439 deviation of the differences was not so large (1.00 ppm), which corresponded to the similar but shifted
440 vertical profiles in shapes between the CO₂ sonde and aircraft measurements as shown in Fig. 8. The
441 difference between the CO₂ sonde data and the NIES/JAXA chartered aircraft data on February 3rd is
442 nearly equal to the difference between CONTRAIL data on February 2nd and the NIES/JAXA
443 chartered aircraft data on February 3rd.

444 Table 3 lists the comparisons of the CO₂ concentrations measured by the balloon CO₂ sonde and
445 CONTRAIL aircraft, 11_060d on January 31st and 11_062d on February 2nd, 2011 up to the altitude
446 of 7,000 m. The averaged values of the aircraft measurements over the range of each balloon altitude
447 ± 200 m are listed in Table 3. The biases between the CO₂ sonde and the CONTRAIL aircraft results
448 were relatively small, 0.33 and 0.35 ppm, and the standard deviations of the differences were 1.16 and
449 1.30 ppm for the results on January 31st and February 3rd, respectively.

450 From the comparison between the CO₂ sonde data and the aircrafts (NIES/JAXA and CONTRAIL)
451 data, it was found that the CO₂ sonde observation was larger than those of aircrafts by about 0.6 ppm
452 on average. The standard deviation of the difference from the CO₂ sonde and aircraft observations was
453 1.2 ppm (1σ). If the 4 sets of aircraft measurement data obtained by the NIES/JAXA and CONTRAIL
454 observations were accurate within the published uncertainties, ignoring the differences in the flight
455 time and geographical routes, the measurement error of the CO₂ sonde system was estimated from the
456 standard deviations of all the difference values in Tables 2 and 3. The estimated error value up to an
457 altitude of 7 km was 0.6 ± 1.2 ppm for the CO₂ sonde observation with a 240 m altitude resolution and
458 3 m s^{-1} ascending speed. The root mean square value (1.3 ppm) from all the difference value in Table
459 2 and 3 indicated that the CO₂ sonde could measure the CO₂ vertical profiles within 1.3 ppm on average
460 compared to the aircraft observations.

461

462 c. CO₂ sonde observations over a forested area

463 Figure 9 shows the vertical profiles of the CO₂ mole fraction, temperature, and relative humidity



464 obtained from the balloon-borne experiments of the CO₂ sonde at Moshiri (44.4°N, 142.3°E) on
465 August 26, 2009. The launch site is in a rural area of Hokkaido, Japan and is surrounded by forests.
466 The CO₂ sonde was launched at 13:29 LST and ascended with a mean vertical speed of approximately
467 3 m s⁻¹. The CO₂ sonde reached an altitude of 10 km after 56 min. The wind horizontally transported
468 the CO₂ sonde distances of 10 km and 21 km northeast when the CO₂ sonde reached the altitudes of 5
469 km and 8 km, respectively. The CO₂ sonde rapidly moved 52 km southeast at an altitude of 16 km.
470 Finally, the CO₂ sonde reached an altitude of 28 km before the balloon burst and the subsequent fall
471 of the sonde was directed by the parachute into the Sea of Okhotsk located 80 km east of the launch
472 site. The error bars for the CO₂ mole fraction in Fig. 9a were calculated from the deviation of the signal
473 intensities from the CO₂ sensor during the 40 s measurement periods for the ambient air and the two
474 standard gases.

475 The vertical temperature profile in Fig. 9b indicated the existence of three inversion layers of the
476 altitudes of approximately 2.0, 3.2, and 4.3 km. The relative humidity from the ground to the first
477 inversion layer at 2.0 km and between the second and third inversion layers from 3.2 to 4.3 km were
478 higher compared with those observed from 2.0 to 3.2 km and from 4.3 to 7.5 km. The CO₂ mole
479 fraction was the lowest near the ground (~373 ppm) and increased to approximately 384 ppm at an
480 altitude of 4–5 km around the third inversion layer before reaching a value of 387 ppm in the upper
481 troposphere (5–9 km). Significant decreases in the CO₂ mole fractions were observed in the two lower
482 layers from the ground to 3.2 km. Considering the clear weather on the day of the balloon experiment,
483 these results are explained by the uptake of CO₂ near the surface by plants in the forests through
484 photosynthesis processes in the daytime hours, and the diffusion and advection of the air mass
485 containing low CO₂ concentrations in the upper altitudes.

486 Because the CO₂ mole fraction for the vertical profiles near the surface is critically important to
487 estimating the flux around the observation point, the vertical profile data taken by our CO₂ sonde is
488 useful.



489

490 **d. CO₂ sonde observations over an urban area**

491 Figure 10 shows the vertical profiles of the CO₂ mole fraction, temperature, and relative humidity
492 obtained by the CO₂ sonde at Moriya (35.93°N, 140.00°E) on February 3rd, 2011. The launching time
493 was 13:10 LST and the sonde ascended with a mean vertical speed of approximately 2.9 m s⁻¹. Moriya
494 is located in the Kanto region and is 40 km northeast of the Tokyo metropolitan area. The launching
495 site was surrounded by the heavy traffic roads and residential areas. As seen in Fig. 10a, high CO₂
496 mole fractions were observed from the ground up to an altitude of 1 km. The average CO₂ volume
497 mole fraction in this layer was higher than that measured in the free troposphere approximately above
498 15 ppm. A small temperature inversion layer appeared at approximately 1 km, and the maximum
499 relative humidity was observed just below this inversion layer (Figs. 10b and c). These results
500 suggested that the CO₂ emitted from anthropogenic sources in and/or around the Tokyo metropolitan
501 area accumulated in the boundary layer at altitudes below 1 km.

502 An analysis of Figs. 9 and 10 indicated that there were a clear local consumption and emission of
503 CO₂ from the comparison of the levels of CO₂ concentration in the free troposphere, which suggested
504 a decoupling with the boundary-layer and synoptic inversion layers (Mayfield and Fochesatto, 2013).
505 When a small increase in a column XCO₂ value is observed by a satellite, it is difficult to estimate
506 which part of the atmosphere is responsible for the increase in XCO₂, the boundary layer with strong
507 CO₂ emission in the nearby area, or the free troposphere. Considering this fact, the vertical profile data
508 obtained by the CO₂ sonde around urban areas should provide more useful information than the column
509 averaged observations obtained by the satellites and FTS measurements to estimate the flux of
510 anthropogenic CO₂ emitted in and/or around the urban areas.

511

512 **4. Conclusion**

513 The CO₂ sonde is shown to be a feasible instrument for CO₂ measurements in the troposphere. The
514 laboratory test with a vacuum chamber has shown the precision of the CO₂ sonde at ~1010 hPa for 0.6



515 ppm and at ~250 hPa for 1.2 ppm. Comparisons of the CO₂ vertical profiles obtained by the CO₂ sonde
516 with two types of aircraft observations, the CONTRAIL and the NIES/JAXA chartered aircraft, were
517 carried out. The CO₂ sonde and CONTRAIL data were consistent. The CO₂ sonde data on January
518 31st, 2011 was in good agreement with the chartered aircraft data on the same day, but the CO₂ sonde
519 data observed on February 3rd, 2011 was larger by approximately 1.4 ppm, as compared with the
520 chartered aircraft data obtained on the same day from the ground to an altitude of 7 km. The
521 measurement errors of the CO₂ sonde system up to an altitude of 7 km were estimated to be 1.4 ppm
522 for a single point of 80 s period measurements with a vertical height resolution of 240–400 m. We
523 conducted the field CO₂ sonde observations more than 20 times in Japan and successfully obtained
524 CO₂ vertical profiles from the ground up to altitudes of approximately 10 km.

525 Our results showed that low-cost CO₂ sondes could potentially be used for frequently measurements
526 of vertical profiles of CO₂ in any parts of the world providing as useful information to understand the
527 global and regional carbon budgets by replenishing the present sparse observation coverage. The CO₂
528 sondes can detect the local and regional transport evidence by determining CO₂ concentrations in the
529 air layer trapped between elevated inversion layers. Also, the CO₂ sonde observation data will help
530 improve the inter-comparison exercise for inverse models and for the partial validation of satellite
531 column integral data. In future, the CO₂ sonde data will be used for the validation of satellites and the
532 calibration of ground-based observations of sunlight spectroscopic measurements for column values
533 of CO₂ concentration.

534

535

536 **Acknowledgments**

537 We would like to thank N. Toriyama, M. Kanada, H. Jindo, M. Sera, H. Sasago, T. Ide, S. Takekawa,
538 M. Kawasaki, G. Inoue (Nagoya Univ.), M. Fujiwara, Y. Inai (Hokkaido Univ.), S. Aoki, and T.
539 Nakazawa (Tohoku Univ.) for their assistance and useful suggestions in the development of CO₂ sonde



540 and the observations. This work was partly supported by the Grant-in-Aid for Scientific Research
541 (KAKENHI 20310008 and 24310012), Green Network of Excellence, Environmental Information
542 (GRENE-ei) program from the Ministry of Education, Culture, Sports, Science and Technology
543 (MEXT), Development of Systems and Technology for Advanced Measurement and Analysis Program
544 from Japan Science and Technology Agency (JST), and the joint research program of the Solar-
545 Terrestrial Environment Laboratory (Now new organization: the Institute for Space-Earth
546 Environmental Research), Nagoya University.
547



548 **References**

- 549 Ahmadov, R., Gerbig, C., Kretschmer, R., Körner, S., Rödenbeck, C., Bousquet, P., and Ramonet,
550 M.: Comparing high resolution WRF-VPRM simulation and two global CO₂ transport models
551 with coastal tower measurements of CO₂, *Biogeosciences*, **6**, 807–817, doi:10.5194/bg-6-807-
552 2009, 2009.
- 553 Andrews, A. E. and Coauthors: CO₂, CO, and CH₄ measurements from tall towers in the NOAA
554 Earth System Research Laboratory's Global Greenhouse Gas Reference Network:
555 instrumentation, uncertainty analysis, and recommendations for future high-accuracy greenhouse
556 gas monitoring efforts, *Atmos. Meas. Tech.*, **7**, 647–687, doi:10.5194/amt-7-647-2014, 2014.
- 557 Baker, D. F. and Coauthors: TransCom 3 inversion intercomparison: Impact of transport model errors
558 on the interannual variability of regional CO₂ fluxes, 1988–2003, *Global Biogeochem. Cycles*, **20**,
559 GB1002, doi:10.1029/2004GB002439, 2006.
- 560 Bakwin, P. S., Tans, P. P., Zhao, C., Ussler III, W., and Quesnell, E.: Measurements of carbon dioxide
561 on a very tall tower, *Tellus* **47B**, 535–549, 1995, doi:10.1034/j.1600-0889.47.issue5.2.x, 2002.
- 562 Chédin, A., Serrar, S., Armante, R., Scott, N. A., and Hollingsworth, A.: Signatures of annual and
563 seasonal variations of CO₂ and other greenhouse gases from comparisons between NOAA TOVS
564 observations and radiation model simulations, *J. Climate*, **15**, 95–116, doi:10.1175/1520-
565 0442(2002)015<0095:SOAASV>2.0.CO;2, 2002.
- 566 Conway, T. J., Tans, P. P., Waterman, L. S., Thoning, K. W., Masarie, K. A., and Gammon, R. H.:
567 Atmospheric carbon dioxide measurements in the remote global troposphere, 1981–1984, *Tellus*
568 *B*, **40**, 81–115, doi:10.1111/j.1600-0889.1988.tb00214.x., 1988.
- 569 Conway, T. J., Tans, P. P., Waterman, L. S., Thoning, K. W., Kitzis, D. R., Masarie, K. A. and Zhang,
570 N.: Evidence for interannual variability of the carbon cycle from the National Oceanic and
571 Atmospheric Administration/Climate Monitoring and Diagnostics Laboratory global air sampling
572 network, *J. Geophys. Res.*, **99**(D11), 22,831–22,855, doi:10.1029/94JD01951, 1994.
- 573 Crevoisier, C., Heilliette, S., Chédin, A., Serrar, S., Armante, R. and Scott, N. A.: Midtropospheric



- 574 CO₂ concentration retrieval from AIRS observations in the tropics, *Geophys. Res. Lett.*, **31**,
575 L17106, doi:10.1029/2004GL020141, 2004.
- 576 Daube, B. C., Boering, K. A., Andrews, A. E. and Wofsy, S. C.: A high-precision fast-response
577 airborne CO₂ analyzer for in situ sampling from the surface to the middle stratosphere, *J.*
578 *Atmospheric Ocean. Technol.*, **19**(10), 1532-1543, doi:10.1175/1520-0426(2002)019
579 <1532:AHPFRA>2.0.CO;2, 2002.
- 580 Dils, B. and Coauthors: Comparisons between SCIAMACHY and ground-based FTIR data for total
581 columns of CO, CH₄, CO₂ and N₂O, *Atmos. Chem. Phys.*, **6**, 1953–1976, doi:10.5194/acp-6-
582 1953-2006, 2006.
- 583 Durry, G., Amarouche, N., Zéninari, V., Parvitte, B., Lebarbu, T. and Ovarlez, J.: In situ sensing of
584 the middle atmosphere with balloon borne near-infrared laser diodes, *Spectrochimica Acta Part A*,
585 **60**, 3371–3379, doi:10.1016/j.saa.2003.11.050, 2004.
- 586 Eldering, A. and Coauthors: The Orbiting Carbon Observatory-2: first 18 months of science data
587 products, *Atmos. Meas. Tech.*, **10**, 549-563, doi:10.5194/amt-10-549-2017, 2017.
- 588 Fang, S. X., Zhou, L. X., Tans, P. P., Ciais, P., Steinbacher, M., Xu, L., and Luan, T.: In situ
589 measurement of atmospheric CO₂ at the four WMO/GAW stations in China, *Atmos. Chem. Phys.*,
590 **14**, 2541–2554, doi:10.5194/acp-14-2541-2014, 2014.
- 591 Gurney, K. R. and Coauthors: Towards robust regional estimates of CO₂ sources and sinks using
592 atmospheric transport models, *Nature*, **415**, 626-630, doi:10.1038/415626a, 2002.
- 593 Gurney, K. R. and Coauthors: Transcom 3 inversion intercomparison: Model mean results for the
594 estimation of seasonal carbon sources and sinks. *Global Biogeochem. Cycles*, **18**, GB1010,
595 doi:10.1029/2003GB002111, 2004.
- 596 Ghysels, M., Durry, G., Amarouche, N., Cousin, J., Joly, L., Riviere, E. D., and Beaumont, L.: A
597 lightweight balloon-borne laser diode sensor for the in situ measurement of CO₂ at 2.68 micron in
598 the upper troposphere and the lower stratosphere, *Appl. Phys. B*, **107**(1), 213-220,



- 599 doi:10.1007/s00340-012-4887-y, 2012.
- 600 Hodgkinson, J., Smith, R., Ho, Wah On, Saffell, J. R., Tatam, R. P.: Non-dispersive infra-red (NDIR)
601 measurement of carbon dioxide at 4.2 μm in a compact and optically efficient sensor, *Sensors and*
602 *Actuators B*, **186**, 580–588. doi: 10.1016/j.snb.2013.06.006, 2013.
- 603 Inai Y., Aoki, S., Honda, H., Furutani, H., Matsumi, Y., Ouchi, M., Sugawara, S., Hasebe, F.,
604 Uematsu, M., Fujiwara, M.: Balloon-borne tropospheric CO₂ observations over the equatorial
605 eastern and western Pacific, *Atmos. Env.*, **184**, 24-36. doi: 10.1016/j.atmosenv.2018.04.016, 2018.
- 606 Inoue, H. Y., and Matsueda, H.: Measurements of atmospheric CO₂ from a meteorological tower in
607 Tsukuba, Japan. *Tellus*, **53B**, 205–219, doi:10.1034/j.1600-0889.2001.01163.x, 2001.
- 608 Joly, L., Parvitte, B., Zeninari, V. and Durry, G.: Development of a compact CO₂ sensor open to the
609 atmosphere and based on near-infrared laser technology at 2.68 μm , *Appl. Phys. B*, **86**, 743–748,
610 doi:10.1007/s00340-006-2568-4, 2007.
- 611 Karion, A., C. Sweeney, P. Tans, and T. Newberger, 2010: AirCore: An innovative atmospheric
612 sampling system, *J. Atmos. Oceanic Technol.*, **27**, 1839–1853, doi:10.1175/2010JTECHA1448.1.
- 613 Komhyr, W. D., Harris, T. B., Waterman, L. S., Chin, J. F. S. and Thoning, K. W.: Atmospheric
614 carbon dioxide at Mauna Loa Observatory 1. NOAA global monitoring for climatic change
615 measurements with a nondispersive infrared analyzer, 1974–1985, *J. Geophys. Res.*, **94**, 8533–
616 8547, doi:10.1029/JD094iD06p08533, 1989.
- 617 Machida, T., Matsueda, H., Sawa, Y., Nakagawa, Y., Hirotsu, K., Kondo, N., Goto, K., Ishikawa, K.,
618 Nakazawa, T., and Ogawa, T.: Worldwide measurements of atmospheric CO₂ and other trace gas
619 species using commercial airlines, *J. Atmos. Oceanic Technol.*, **25**(10), 1744–1754,
620 doi:10.1175/2008JTECHA1082.1, 2008.
- 621 Maksyutov, S., Nikolay, K., Nakatsuka, Y., Patra, P. K., Nakazawa, T., Yokota, T., and Inoue, G.:
622 Projected Impact of the GOSAT observations on regional CO₂ flux estimations as a function of
623 total retrieval error. *J. Remote Sensing Soc. Japan*, **28**, 190-197, doi:10.11440/rssj.28.190, 2008.



- 624 Matsueda, H., Machida, T., Sawa, Y., Nakagawa, Y., Hirotsu, K., Ikeda, H., Kondo, N., and Goto,
625 K.: Evaluation of atmospheric CO₂ measurements from new flask air sampling of JAL airliner
626 observations. *Pap. Meteor. Geophys.*, **59**, 1–17, doi:10.2467/mripapers.59.1, 2008.
- 627 Mayfield J. A. and Fochesatto, G. J.: The Layered Structure of the winter Atmospheric Boundary Layer in the
628 Interior of Alaska. *J. Appl. Met. Climatol.*, **52**, 953–973, doi.org/10.1007/s00703-013-0274-4, 2013.
- 629 Morino, I. and Coauthors, 2011: Preliminary validation of column-averaged volume mixing ratios of
630 carbon dioxide and methane retrieved from GOSAT short-wavelength infrared spectra, *Atmos.*
631 *Meas. Tech.*, **4**, 1061–1076, doi:10.5194/amt-4-1061-2011.
- 632 Nakazawa, T., Murayama, S., Miyashita, K., Aoki, S., and Tanaka, M.: Longitudinally different
633 variations of lower tropospheric carbon dioxide concentrations over the North Pacific Ocean,
634 *Tellus*, **44B**, 161–172, doi:10.3402/tellusb.v44i3.15438, 1992
- 635 Nakazawa, T., Machida, T., Sugawara, S., Murayama, S., Morimoto, S., Hashida, G., Honda, H. and
636 Itoh, T.: Measurements of the stratospheric carbon dioxide concentration over Japan using a
637 balloon-borne cryogenic sampler, *Geophys. Res. Letter*, **22**, 1229–1232, doi:10.1029/95GL01118,
638 1995.
- 639 Pales, J. C., and Keeling, C. D.: The concentration of atmospheric carbon dioxide in Hawaii, J.
640 *Geophys. Res.*, **70**(24), 6053–6076, doi:10.1029/JZ070i024p06053, 1965.
- 641 Stephens, B. B. and Coauthors: Weak northern and strong tropical land carbon uptake from vertical
642 profiles of atmospheric CO₂, *Science*, **316**, 1732–1735, doi:10.1126/science.1137004, 2007.
- 643 Sweeney, C. and Coauthors: Seasonal climatology of CO₂ across North America from aircraft
644 measurements in the NOAA/ESRL Global Greenhouse Gas Reference Network, *J. Geophys. Res.*,
645 **120**, 5155–5190, doi:10.1002/2014JD022591, 2014.
- 646 Tanaka, M., Nakazawa, T. and Aoki, S.: High quality measurements of the concentration of
647 atmospheric carbon dioxide. *J. Meteor. Soc. Japan*, **61**, 678–685, doi:10.2151/jmsj1965.61.4_678,
648 1983.



- 649 Tanaka, M., Nakazawa, T. and Aoki S.: Time and space variations of tropospheric carbon dioxide
650 over Japan, *Tellus*, **39B**, 3–12, doi:10.3402/tellusb.v39i1-2.15318, 1987.
- 651 Tanaka, T., Miyamoto, Y., Morino, I., Machida, T., Nagahama, T., Sawa, Y., Matsueda, H., Wunch,
652 D., Kawakami, S., and Uchino, O.: Aircraft measurements of carbon dioxide and methane for the
653 calibration of ground-based high-resolution Fourier Transform Spectrometers and a comparison to
654 GOSAT data measured over Tsukuba and Moshiri. *Atmos. Meas. Tech.*, **5**, 2003–2012,
655 doi:10.5194/amt-5-2003-2012, 2012.
- 656 Tans, P. P., Conway, T., and Nakazawa T.: Latitudinal distribution of the sources and sinks of
657 atmospheric carbon dioxide derived from surface observations and an Atmospheric Transport
658 Model, *J. Geophys. Res.*, **94**, 5151–5172, doi:10.1029/JD094iD04p05151, 1989.
- 659 Watai, T., Machida, T., Ishizaki, N. and Inoue, G.: A lightweight observation system for atmospheric
660 carbon dioxide concentration using a small unmanned aerial vehicle, *J. Atmos. Oceanic Technol.*,
661 **23**, 700–710 doi:10.1175/JTECH1866.1, 2006.
- 662 Winderlich, J., Chen, H., Gerbig, C., Seifert, T., Kolle, O., Lavrič, J. V., Kaiser, C., Höfer, A., and
663 Heimann, M.: Continuous low-maintenance CO₂/CH₄/H₂O measurements at the Zotino Tall
664 Tower Observatory (ZOTTO) in Central Siberia, *Atmos. Meas. Tech.*, **3**, 1113–1128,
665 doi:10.5194/amt-3-1113-2010, 2010.
- 666 WMO: The state of greenhouse gases in the atmosphere using global observations through 2015,
667 WMO Greenhouse Gas Bull., **12**, 1–8, 2016.
- 668 Wofsy, S. C., the HIPPO science team and cooperating modellers and satellite teams: HIAPER Pole-
669 to-Pole Observations (HIPPO): fine-grained, global-scale measurements of climatically important
670 atmospheric gases and aerosols, *Phil. Trans. R. Soc. A*, **369**, 2073–2086,
671 doi:10.1098/rsta.2010.0313, 2011.
- 672 Wunch, D., Toon, G. C., Blavier, J. L., Washenfelder, R. A., Notholt, J., Connor, B. J., Griffith, D. W.
673 T., Sherlock, V. and Wennberg, P. O.: The Total Carbon Column Observing Network. *Phil. Trans.*



- 674 R. Soc. A, **369**, 2087–2112, doi:10.1098/rsta.2010.0240, 2011.
- 675 Yokota, T., Yoshida, Y., Eguchi, N., Ota, Y., Tanaka, T., Watanabe, H. and Maksyutov, S.: Global
676 concentrations of CO₂ and CH₄ retrieved from GOSAT: First preliminary results, Sci. Online Lett.
677 Atmos., **5**, 160–163, doi:10.2151/sola.2009–041, 2009.
- 678 Yoshida, Y., Ota, Y., Eguchi, N., Kikuchi, N., Nobuta, K., Tran, H., Morino, I., and Yokota, T.:
679 Retrieval algorithm for CO₂ and CH₄ column abundances from short-wavelength infrared spectral
680 observations by the Greenhouse gases observing satellite, Atmos. Meas. Tech., **4**, 717–734,
681 doi:10.5194/amt-4-717-2011, 2011.
- 682



683 **Table 1.** CONTRAIL flight data near to the CO₂ sonde measurements on 31 January and 3 February

684 2011.

685

686

Data set name	Date	Time (LST) ^a
11_057a	CONTRAIL (29 January)	19:01
11_058d	CONTRAIL (30 January)	15:06
11_059a	CONTRAIL (30 January)	18:46
11_060d	CONTRAIL (31 January)	15:07
11_061a	CONTRAIL (1 February)	18:46
11_062d	CONTRAIL (2 February)	14:58
11_063a	CONTRAIL (4 February)	18:58
	CO ₂ sonde (31 January)	13:06
	CO ₂ sonde (3 February)	13:10

687

688 ^a Time for the CONTRAIL data represents the flight time in Japan Standard Time at an altitude of 1

689 km over the Narita airport. Time for the CO₂ sonde data represents the launching time at Moriya.

690

691

692



693 **Table 2.** Comparisons of the CO₂ concentrations between the balloon CO₂ sonde and NIES/JAXA
 694 chartered aircraft measurements on 31st January and 3rd February 2011.

695

JAXA-NIES Chartered Aircraft (31 January 2011)				JAXA-NIES Chartered Aircraft (3 February 2011)			
Altitude (m) ^a	Balloon CO ₂ (ppm)	Aircraft CO ₂ (ppm) ^b	Difference (ppm) ^c	Altitude (m) ^a	Balloon CO ₂ (ppm)	Aircraft CO ₂ (ppm) ^b	Difference (ppm) ^c
849	399.05	397.62	1.43	1324	396.60	394.45	2.15
1202	398.16	397.53	0.63	1612	394.65	393.03	1.62
1610	398.00	397.17	0.83	1917	394.86	394.10	0.76
2038	396.50	396.95	-0.45	2223	395.77	393.54	2.23
2291	398.03	396.04	1.99	2539	395.41	393.95	1.45
2463	396.54	395.65	0.89	2867	394.71	395.11	-0.40
2844	393.44	395.24	-1.79	3215	394.99	392.99	2.00
3329	395.45	394.15	1.30	3543	393.59	393.07	0.52
3732	393.51	393.63	-0.12	3764	393.69	393.40	0.28
4161	395.47	393.54	1.93	3938	395.15	393.11	2.04
4575	394.62	392.94	1.68	4169	393.83	392.68	1.15
4918	393.24	393.64	-0.41	4458	396.57	393.51	3.06
5273	392.41	393.25	-0.84	4750	394.88	393.69	1.19
5654	393.02	393.47	-0.45	5047	396.53	394.01	2.53
6083	391.87	392.91	-1.04	5214	395.91	393.45	2.46
6510	392.76	391.65	1.11	5383	396.78	393.58	3.20
		Average =	0.42	5565	395.83	393.67	2.15
		Std Dev ^d =	1.16	5781	395.18	393.39	1.80
		RMS ^e =	1.20	6092	391.75	392.83	-1.09
				6287	392.44	392.42	0.02
				6467	393.67	392.23	1.44
				6639	395.07	392.42	2.65
				6815	394.00	393.00	1.00
						Average =	1.41
						Std Dev ^d =	1.00
						RMS ^e =	1.62

696 a. Altitudes of the balloon-borne experiments using the in-flight calibration with 40-s time intervals.

697 b. Averaged values of the aircraft measurement results over the range of the balloon altitudes ± 100 m.

698 c. Difference values of [balloon CO₂] - [Aircraft CO₂]

699 d. Standard deviation of the differences (1σ).

700 e. Root mean square values.

701



702 **Table 3.** Comparisons of the CO₂ concentrations between the balloon CO₂ sonde measurements on
 703 31 January and CONTRAIL aircraft CME on 31 January (11_060d) and between the CO₂ sonde on 3
 704 February and CONTRAIL on 2 February (11_062d) up to the altitude of 7 km. The annotations are
 705 same as Table 2.
 706

CONTRAIL 11_060d (31 January 2011)				CONTRAIL 11_062d (2 February 2011)			
Altitude (m)	Balloon CO ₂ (ppm)	Aircraft CO ₂ (ppm)	Difference (ppm)	Altitude (m)	Balloon CO ₂ (ppm)	Aircraft CO ₂ (ppm)	Difference (ppm)
849	399.05	398.21	0.84	1917	394.86	396.59	-1.73
1202	398.16	399.56	-1.40	2223	395.77	396.45	-0.68
1610	398.00	398.77	-0.76	2539	395.41	395.71	-0.30
2038	396.50	397.07	-0.57	2867	394.71	394.67	0.04
2291	398.03	395.97	2.06	3215	394.99	393.34	1.65
2463	396.54	394.55	1.99	3543	393.59	394.25	-0.66
2844	393.44	393.41	0.04	3764	393.69	394.33	-0.64
3329	395.45	394.25	1.20	3938	395.15	394.69	0.46
3732	393.51	393.58	-0.07	4458	396.57	394.09	2.48
4161	395.47	393.86	1.61	4750	394.88	395.02	-0.14
4575	394.62	393.18	1.44	5047	396.53	396.55	-0.01
4918	393.24	393.62	-0.38	5214	395.91	396.01	-0.10
5273	392.41	392.76	-0.35	5383	396.78	394.78	2.00
6866	392.31	393.26	-0.96	5565	395.83	393.69	2.14
		Average =	0.33	5781	395.18	393.79	1.39
		Std Dev =	1.16	6092	391.75	393.57	-1.82
		RMS =	1.17	6287	392.44	393.32	-0.88
				6467	393.67	392.89	0.78
				6639	395.07	392.84	2.23
				6815	394.00	393.11	0.90
						Average =	0.35
						Std Dev =	1.30
						RMS =	1.31

707

708



709 **Figure captions**

710 **Figure 1.** Left: Schematic diagram of the CO₂ measurement package, where F1 and F2 represent the
711 band-pass filters at wavelengths of 4.0 μm and 4.3 μm, respectively. The outlet port of the CO₂ sensor
712 is opened to ambient air. Details of the system are described in the text. Right: Photograph of the inside
713 of the CO₂ sonde package. The components were placed in a specially modeled expanded polystyrene
714 box.

715 **Figure 2.** Photograph of the CO₂ sonde developed in this study before launching. a. CO₂
716 measurement package is shown in Fig. 1, b. GPS sonde, and c. Calibration gas package.

717 **Figure 3.** Raw data obtained by the CO₂ sonde launched on September 26, 2011 at Moriya, Japan. The
718 vertical axis is the difference between the 4.0 μm and 4.3 μm signal intensities divided by the ambient
719 pressure. The black line indicates the observation results during the balloon flight with calibration
720 cycles. The red circle indicates the 30 s average values in each step of the calibration. Red curve
721 indicates the cubic spline fitting curves for the observation points of the 30 s average values of the
722 same standard gas. The small black dots on the cubic spline curves indicate the estimated values for
723 the standard gases at the ambient gas measuring timing, which were is used for the interpolation to
724 determine the ambient air concentrations.

725 **Figure 4.** $[I(4.0) - I(4.3)]/P$ values versus CO₂ mole fraction, where $I(4.0)$ and $I(4.3)$ are the
726 signal intensities at the 4.0 μm wavelength for background measurements and the 4.3 μm wavelength
727 for CO₂ absorption measurements, obtained by the NDIR CO₂ sensor, and P is the ambient
728 atmospheric pressure. CO₂ mole fractions were measured with a standard NDIR instrument (LICOR,
729 LI-840A) connected to the balloon sensor in series. The pressure while carrying out the
730 measurements was constant at 1010 hPa.

731 **Figure 5.** Results of a chamber experiment of the CO₂ sonde. Pressure in the chamber was reduced
732 from 1010 hPa (ground level pressure) to 250 hPa (about 10 km altitude pressure) at a temperature of
733 about 298 K. The black circles indicate the value of the CO₂ mole fraction of the sample air in the



734 chamber, which was obtained from the interpolation of the standard gas values in each calibration
735 cycle. Vertical error bars indicate the square-root of sum of squares for the standard deviations of
736 the sample and standard gas signals at each step in the calibration cycle. The black dashed line shows
737 an average of all the values obtained for the sample gas. See the text for more details.

738 **Figure 6.** Flight paths of the CO₂ sonde observations launched at Moriya on January 31st (blue solid
739 line) and February 3rd (red solid line), 2011, the CONTRAIL 11_060d data on January 31st, 2011
740 (black solid line) and 11_062d data on February 2nd, 2011 (black dashed line) from Hong Kong to
741 Narita, and the NIES/JAXA chartered aircraft experiment on January 31st (green solid line) and
742 February 3rd (purple dotted line). The altitudes of the flight paths are also indicated.

743 **Figure 7.** The CO₂ vertical profiles obtained by the CO₂ sonde (circles connected with blue lines),
744 NIES/JAXA chartered aircraft data (dots connected with green lines), and the CONTRAIL data
745 (diamonds connected with black lines) on January 31st, 2011.

746 **Figure 8.** The CO₂ vertical profiles obtained by the CO₂ sonde (circles connected with red lines),
747 NIES/JAXA chartered aircraft data (dots connected with purple lines) on February 3rd, and
748 CONTRAIL data (diamonds connected with black lines) on February 2nd, 2011.

749 **Figure 9.** Profiles of (a) CO₂ mole fraction, (b) temperature (solid line) and potential temperature
750 (dotted line), and (c) relative humidity observed over a forest area, Moshiri in Hokkaido, Japan by
751 the balloon launched on August 26, 2009 at 13:30 (LST). The black circles with error bars in panel
752 (a) represent the data obtained by the CO₂ sonde.

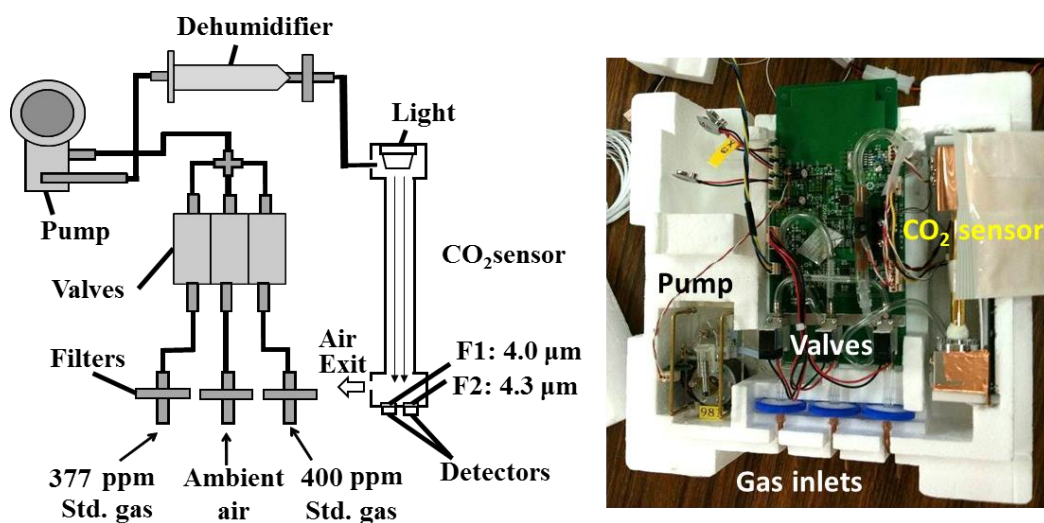
753 **Figure 10.** Profiles of (a) CO₂ mole fraction, (b) temperature (solid line) and potential temperature
754 (dotted line), and (c) relative humidity observed over an urban area, Moriya near Tokyo on February
755 3rd, 2011 at 13:10 (LST).

756

757



758



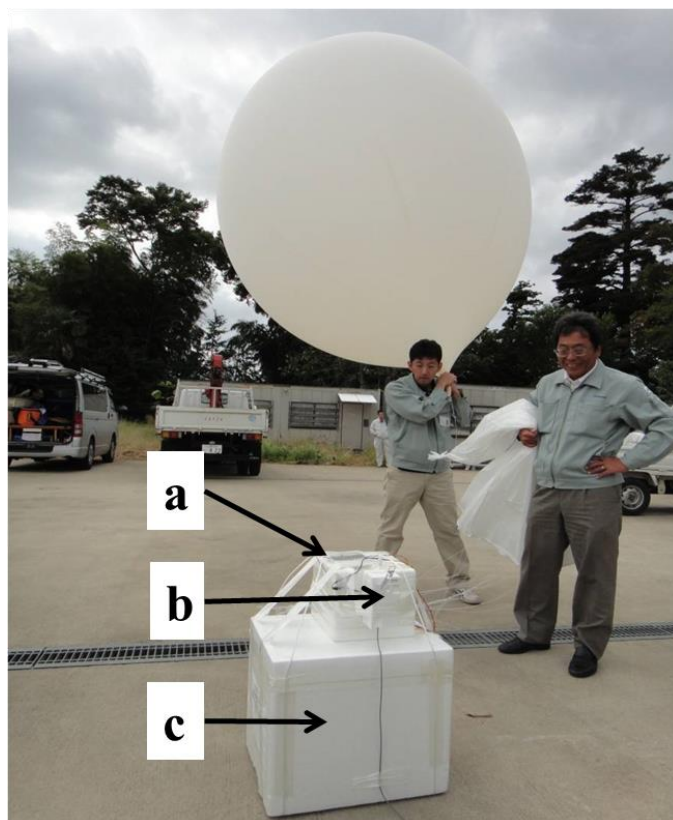
759

760 **Figure 1.** Left: Schematic diagram of the CO₂ measurement package, where F1 and F2 represent the
761 band-pass filters at wavelengths of 4.0 μm and 4.3 μm, respectively. The outlet port of the CO₂ sensor
762 is opened to ambient air. Details of the system are described in the text. Right: Photograph of the inside
763 of the CO₂ sonde package. The components were placed in a specially modeled expanded polystyrene
764 box.

765



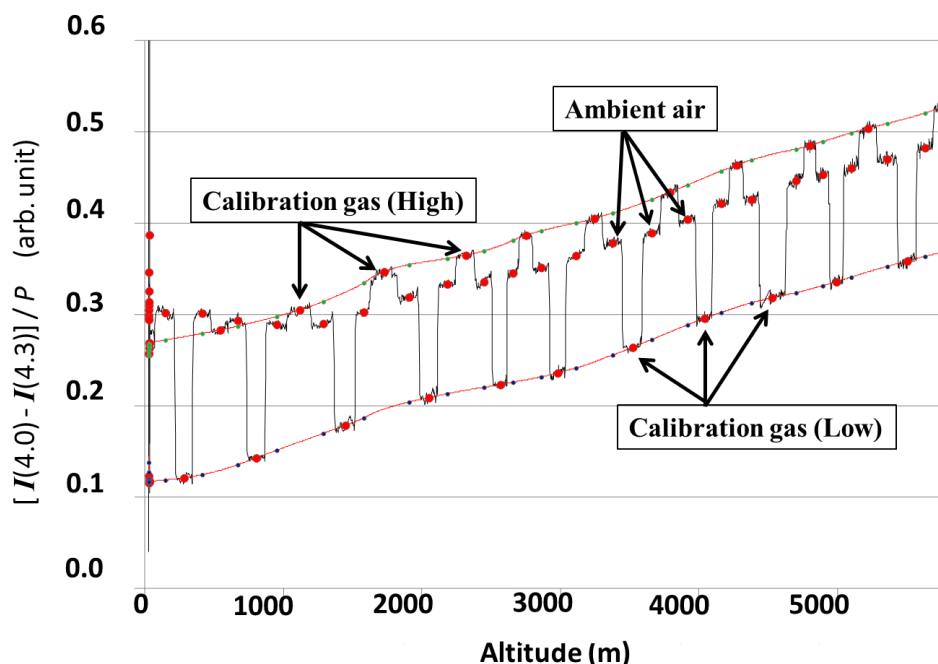
766



767

768 **Figure 2.** Photograph of the CO₂ sonde developed in this study before launching. a. CO₂
769 measurement package is shown in Fig. 1, b. GPS sonde, and c. Calibration gas package.

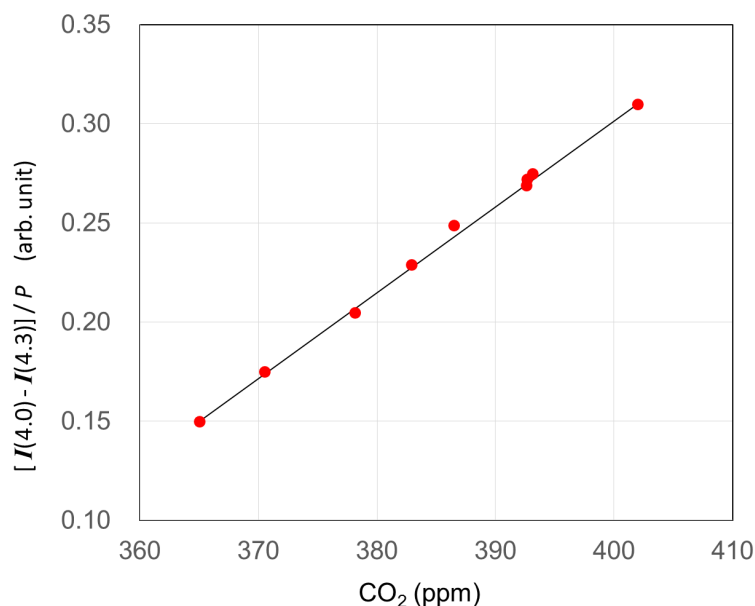
770



771 **Figure 3.** Raw data obtained by the CO₂ sonde launched on September 26, 2011 at Moriya, Japan.
 772 The vertical axis is the difference between the 4.0 μm and 4.3 μm signal intensities divided by the
 773 ambient pressure. The black line indicates the observation results during the balloon flight with
 774 calibration cycles. The red circle indicates the 30 s average values in each step of the calibration. Red
 775 curve indicates the cubic spline fitting curves for the observation points of the 30 s average values of
 776 the same standard gas. The small black dots on the cubic spline curves indicate the estimated values
 777 for the standard gases at the ambient gas measuring timing, which were is used for the interpolation
 778 to determine the ambient air concentrations.
 779
 780



781

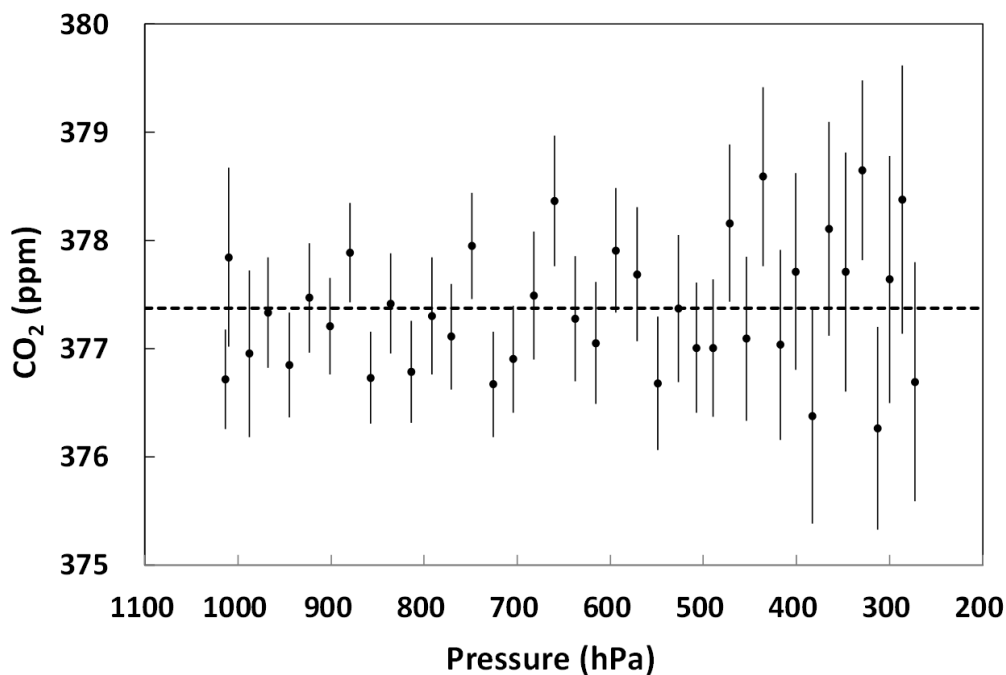


782

783 **Figure 4.** $[I(4.0) - I(4.3)]/P$ values versus CO₂ mole fraction, where $I(4.0)$ and $I(4.3)$ are the
784 signal intensities at the 4.0 μm wavelength for background measurements and the 4.3 μm wavelength
785 for CO₂ absorption measurements, obtained by the NDIR CO₂ sensor, and P is the ambient
786 atmospheric pressure. CO₂ mole fractions were measured with a standard NDIR instrument (LICOR,
787 LI-840A) connected to the balloon sensor in series. The pressure while carrying out the
788 measurements was constant at 1010 hPa.

789

790



791

792

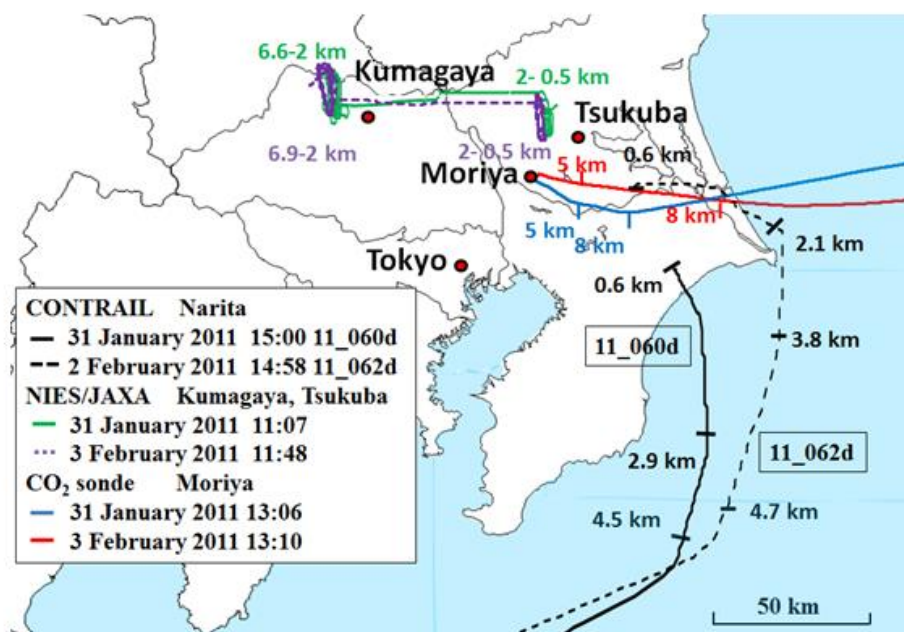
793 **Figure 5.** Results of a chamber experiment of the CO₂ sonde. Pressure in the chamber was reduced
 794 from 1010 hPa (ground level pressure) to 250 hPa (about 10 km altitude pressure) at a temperature of
 795 about 298 K. The black circles indicate the value of the CO₂ mole fraction of the sample air in the
 796 chamber, which was obtained from the interpolation of the standard gas values in each calibration
 797 cycle. Vertical error bars indicate the square-root of sum of squares for the standard deviations of
 798 the sample and standard gas signals at each step in the calibration cycle. The black dashed line shows
 799 an average of all the values obtained for the sample gas. See the text for more details.

800

801

802

803

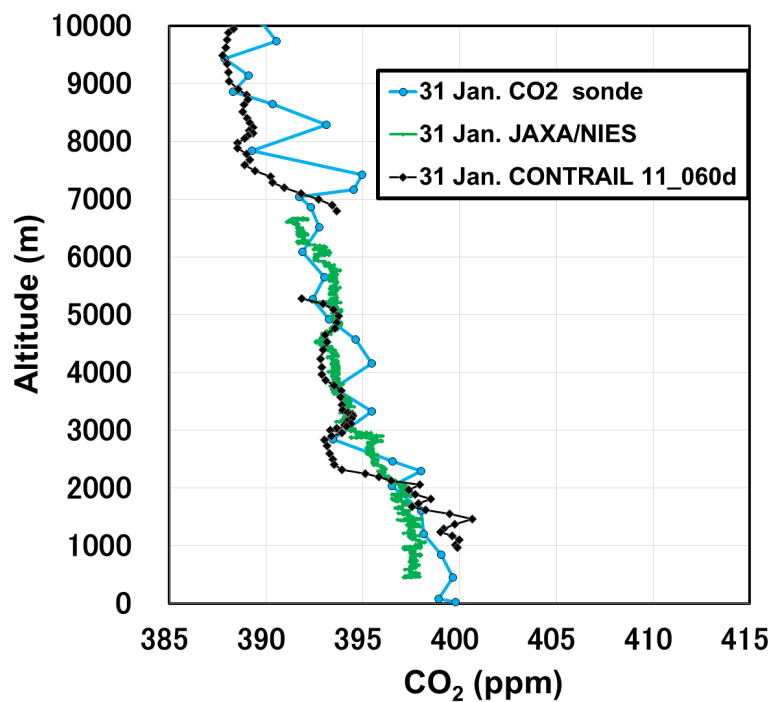


804

805

806 **Figure 6.** Flight paths of the CO₂ sonde observations launched at Moriya on January 31st (blue solid
807 line) and February 3rd (red solid line), 2011, the CONTRAIL 11_060d data on January 31st, 2011
808 (black solid line) and 11_062d data on February 2nd, 2011 (black dashed line) from Hong Kong to
809 Narita, and the NIES/JAXA chartered aircraft experiment on January 31st (green solid line) and
810 February 3rd (purple dotted line). The altitudes of the flight paths are also indicated.

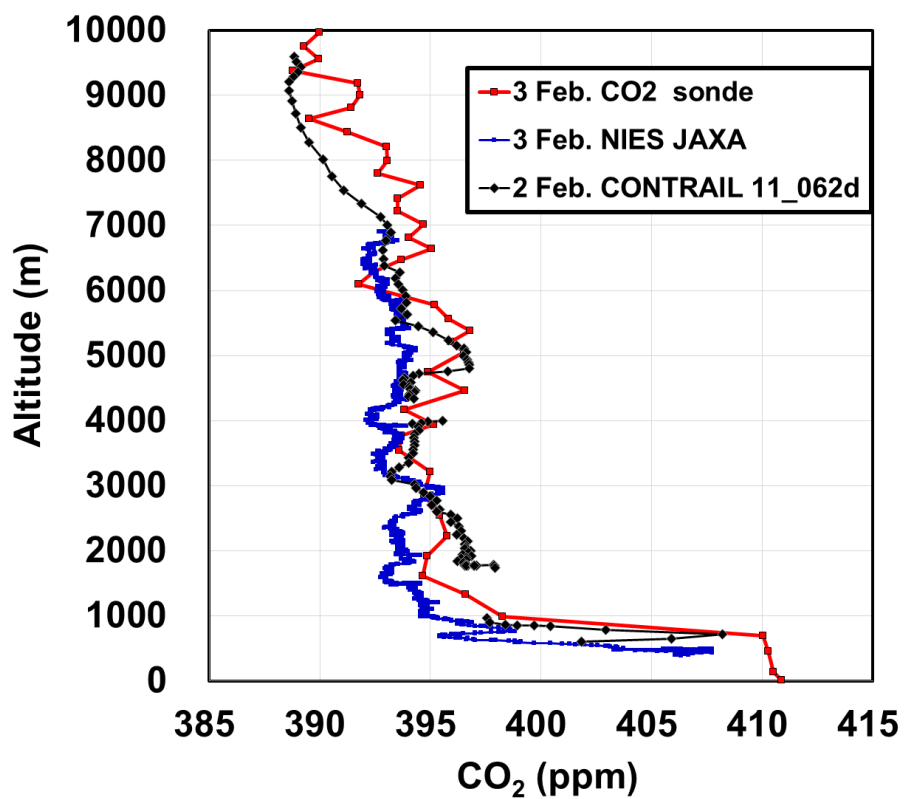
811



812

813 **Figure 7.** The CO₂ vertical profiles obtained by the CO₂ sonde (circles connected with blue lines),
814 NIES/JAXA chartered aircraft data (dots connected with green lines), and the CONTRAIL data
815 (diamonds connected with black lines) on January 31st, 2011.

816



817

818

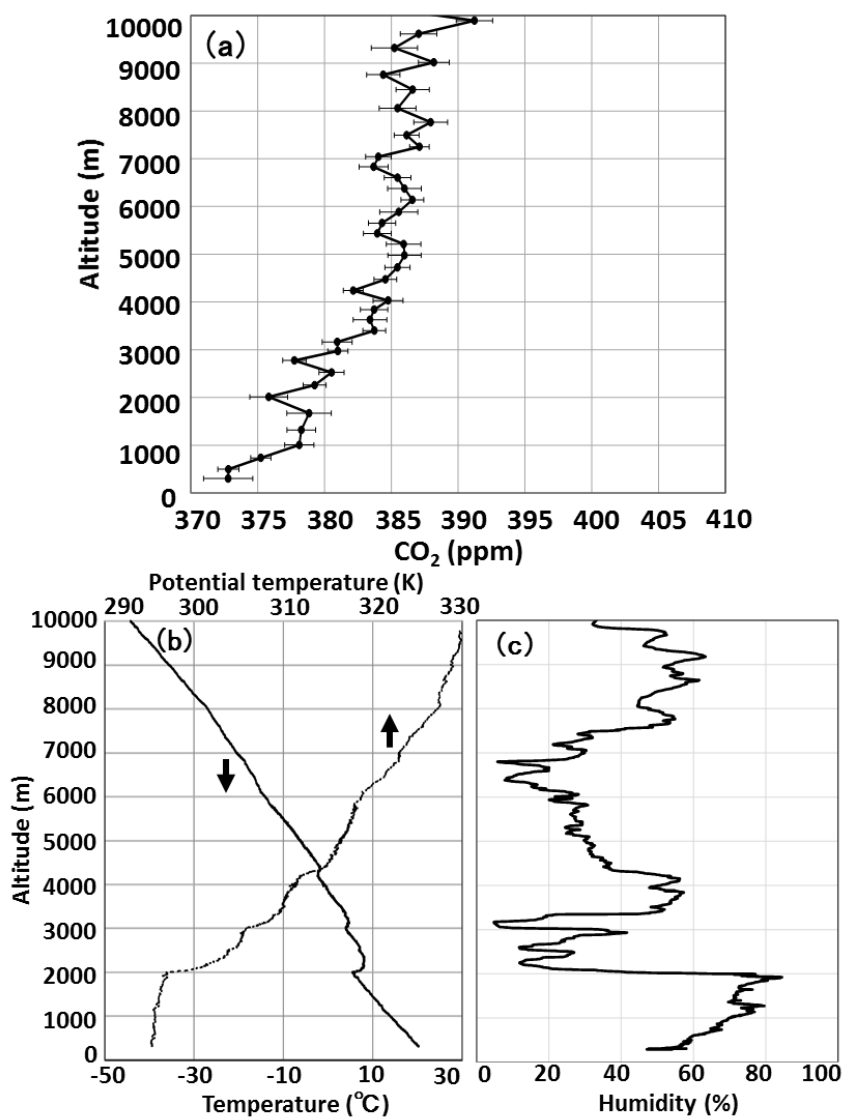
819 **Figure 8.** The CO₂ vertical profiles obtained by the CO₂ sonde (circles connected with red lines),

820 NIES/JAXA chartered aircraft data (dots connected with purple lines) on February 3rd, and

821 CONTRAIL data (diamonds connected with black lines) on February 2nd, 2011.



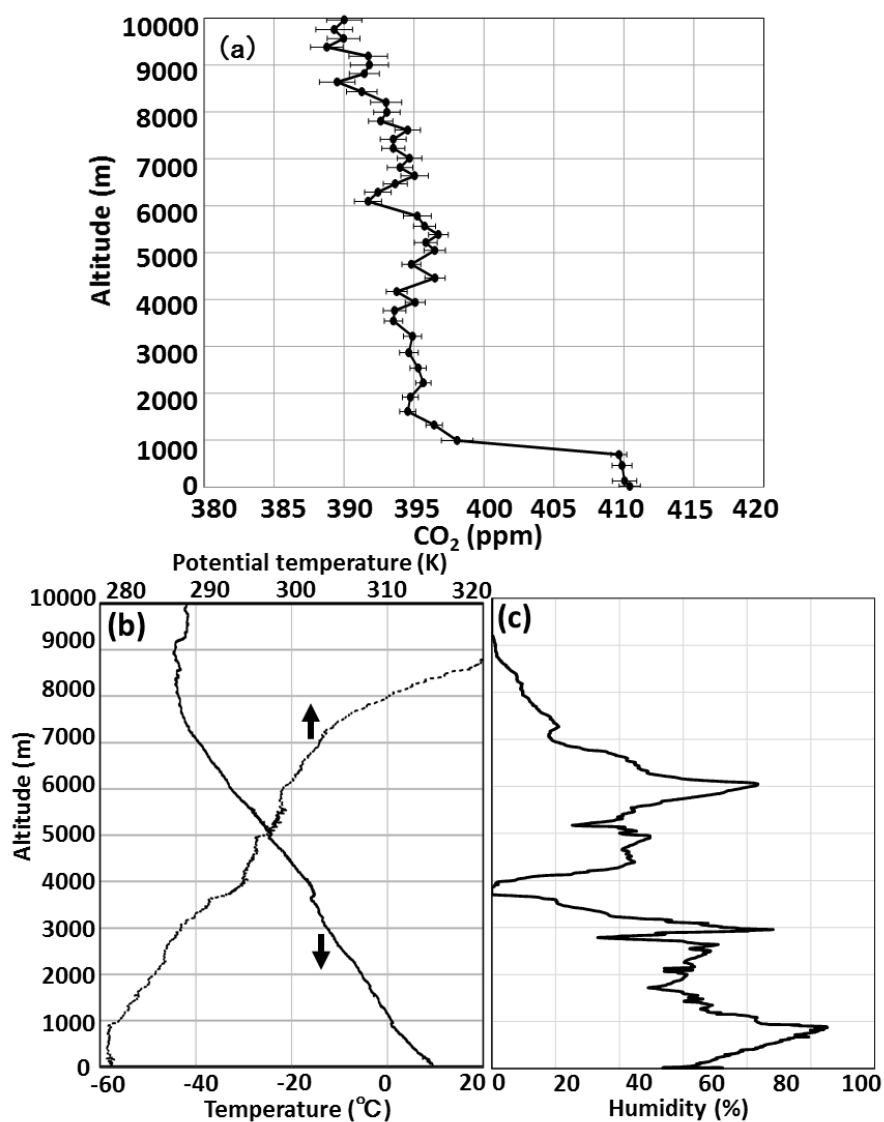
822



823

824 **Figure 9.** Profiles of (a) CO₂ mole fraction, (b) temperature (solid line) and potential temperature
825 (dotted line), and (c) relative humidity observed over a forest area, Moshiri in Hokkaido, Japan by
826 the balloon launched on August 26, 2009 at 13:30 (LST). The black circles with error bars in panel
827 (a) represent the data obtained by the CO₂ sonde.

828



829 **Figure 10.** Profiles of (a) CO₂ mole fraction, (b) temperature (solid line) and potential temperature
830 (dotted line), and (c) relative humidity observed over an urban area, Moriya near Tokyo on February
831 3rd, 2011 at 13:10 (LST).
832